Article

Wear Behavior Analysis of Al$_2$O$_3$ Coatings Manufactured by APS and HVOF Spraying Processes Using Powder and Suspension Feedstocks

Monika Michalak [1,*], Paweł Sokołowski [1], Mirosław Szala [2], Mariusz Walczak [2], Leszek Łatka [1], Filofteia-Laura Toma [3] and Stefan Björklund [4]

1   Faculty of Mechanical Engineering, Wrocław University of Science and Technology, Łukasiewicza 5, 50-371 Wrocław, Poland; pawel.sokolowski@pwr.edu.pl (P.S.); leszek.latka@pwr.edu.pl (L.Ł.)
2   Department of Materials Engineering, Faculty of Mechanical Engineering, Lublin University of Technology, Nadbystrzycka 36D, 20-618 Lublin, Poland; m.szala@pollub.pl (M.S.); m.walczak@pollub.pl (M.W.)
3   Fraunhofer Institute for Material and Beam Technology IWS, Thermal Spraying Group, Winterbergstrasse 28, 01277 Dresden, Germany; Filofteia-Laura.Toma@iws.fraunhofer.de
4   Department of Engineering Science, University West, Gustava Melins, gata 2, 46132 Trollhättan, Sweden; stefan.bjorklund@hv.se
*   Correspondence: monika.michalak@pwr.edu.pl

Abstract: Thermally sprayed ceramic coatings are applied for the protection of surfaces that are exposed mainly to wear, high temperatures, and corrosion. In recent years, great interest has been garnered by spray processes with submicrometric and nanometric feedstock materials, due to the refinement of the structure and improved coating properties. This paper compares the microstructure and tribological properties of alumina coatings sprayed using conventional atmospheric plasma spraying (APS), and various methods that use finely grained suspension feedstocks, namely, suspension plasma spraying (SPS) and suspension high-velocity oxy-fuel spraying (S-HVOF). Furthermore, the suspension plasma-sprayed Al$_2$O$_3$ coatings have been deposited with radial (SPS) and axial (A-SPS) feedstock injection. The results showed that all suspension-based coatings demonstrated much better wear resistance than the powder-sprayed ones. S-HVOF and axial suspension plasma spraying (A-SPS) allowed for the deposition of the most dense and homogeneous coatings. Dense-structured coatings with low porosity (4 vol.%) and good cohesion to the metallic substrate, containing a high content of α–Al$_2$O$_3$ phase (56 vol.%) and a very low wear rate (0.2 ± 0.04 mm$^3 \times 10^{-6}$/(N·m)), were produced with the S-HVOF method. The wear mechanism of ceramic coatings included the adhesive wear mode supported by the fatigue-induced material delamination. Moreover, the presence of wear debris and tribofilm was confirmed. Finally, the coefficient of friction for the coatings was in the range between 0.44 and 0.68, with the highest values being recorded for APS sprayed coatings.

Keywords: Al$_2$O$_3$; coating; atmospheric plasma spraying; suspension plasma spraying; suspension high-velocity oxy-fuel spraying; microstructure; wear behavior; friction coefficient

1. Introduction

The development of highly advanced spray torches and a better understanding of coating deposition mechanisms have contributed to rapid progress in surface engineering [1]. Requirements in many fields of machine operation and production techniques led to applications for various alumina-based coatings, for example, as electrically insulating or wear-protection layers [2]. Such coatings are primarily found in the machinery, marine, chemical, food, textile, printing, and energy industries [3–5].

One of the primary methods of ceramic coating manufacturing is atmospheric plasma spraying (APS) [6] and high-velocity oxy-fuel spraying (HVOF) [7]. Plasma spraying involves the use of a high-temperature plasma jet to produce wear- and erosion-resistant ceramic [8,9], composite [10,11], or metallic coatings [12]. The APS process uses a powder

feedstock (i.e., $-45 + 10$ μm) and results in a relatively coarse-structured coating [13]. In turn, the HVOF technique is characterized by high kinetic energy, relatively low temperature, and uses slightly smaller powders (i.e., $-25 + 5$ μm) than in APS [14]. It enables the application of coatings with high density, favorable hardness, and increased adhesion [15]. The HVOF technique allows the deposition of ceramic [16,17], metallic [18,19], and cermet [20,21] coatings. In general, it also allows the improvement of the tribological properties, e.g., the abrasion wear resistance of the alumina-based HVOF coatings is reported to be two- to three-fold greater than the APS ones [5].

At the same time, these well-established processes are the bases for newly developed spray techniques, namely, suspension plasma spraying (SPS) and suspension high-velocity oxy-fuel spraying (S-HVOF). These are intended for the refinement and tailoring of the coating microstructure, leading to improved functional properties [22,23]. At present, great attention is given toward the processing of submicrometer, or even nanometer, powders, since many of them provide increased wear resistance, a lower friction coefficient, and better corrosion protection [24]. Thus, utilizing a suspension, which consists of both solid and liquid phases, instead of solely a coarse powder, has now become an attractive alternative for conventional powder-based APS or HVOF spraying [25]. During suspension spraying, the spraying distance and process parameters have to be adapted—the mass of the suspension droplet is up to two orders of magnitude lower than that of the micrometer-sized powder [26]. Thus, the acceleration and heating, as well as the deceleration and cooling processes, are very rapid. To gain the benefits of suspension spraying, attention should be paid to the velocity, trajectory and temperature distribution of the sprayed material. In the field of suspension plasma spraying, the feeding of the suspension material occurs in both an axial and a radial manner [27]. Axial injection increases the enthalpy between the plasma and fine powder, resulting in denser, less defect-free coatings with improved mechanical and tribological properties [28,29]. Nonetheless, because of the high cost of equipment, this axial deposition technique is under investigation by only a few research groups [30–32]. The S-HVOF process, similarly to axial SPS (known hereafter as A-SPS) and conventional HVOF processes, ensures also axial feeding.

It is relevant to note that the low intrinsic hardness of steel components can limit their full engagement in tribological applications [33]. Therefore, the protection or regeneration of components via coating deposition is a fundamental trend in current machine development. Ceramic materials, including Al_2O_3, are very popular in industrial applications. Alumina is characterized by high hardness and good strength, wear, and corrosion resistance, and it does not interact with metals during heating [34,35]. However, the performance of coatings is strongly affected by the deposition process itself and the specific technological spray parameters. Therefore, the proper selection of spray parameters to ensure the coating's resistance to different deterioration processes is an up-to-date research object of many scientific papers [36–39].

The tribological properties of alumina and alumina composite coatings depend on the type of powder used, its size, chemical composition, density, etc. [40,41]. Goel et al. [26] demonstrated that the coefficient of friction of alumina coatings changed from 0.61 to 0.75 with the bigger powder size, while the wear rate increased from 0.04 to 0.55×10^{-3} mm^3/(N·m). Many research groups are focused on the control of wear performance by the variation of spraying parameters. Marcinauskas et al. [33] reported a decrease in wear rate from 5.75×10^{-5} to 4.55×10^{-5} mm^3/(N·m) for alumina coatings, with an increased stand-off distance. Bolelli et al. [23] studied the wear of Al_2O_3 coatings sprayed using powders and suspensions by HVOF and S-HVOF, respectively. They showed that the tribological behavior of the coatings is influenced by the formation of a smooth, thin, and dense surface layer, which proceeds through its delamination and removal. Until now, the characterization of wear behavior was extensively reported for alumina deposited by using APS and HVOF, which cannot represent the tribological properties of suspension-sprayed alumina coatings. Additionally, the comparison of different novel deposition methods, likewise A-SPS and S-HVOF with commercial APS, is still insufficient. Furthermore, for the improvement of

the tribological properties of alumina coatings, it is crucial to comparatively analyze the microstructure and, for example, the wear resistance of coatings deposited by conventional and newly developed suspension spraying techniques.

This study aimed to investigate the morphology, microstructure, and wear resistance under dry friction conditions of Al_2O_3 coatings deposited by different spray techniques, i.e., APS, SPS (with radial suspension injection), A-SPS (with axial suspension injection) and S-HVOF.

2. Materials and Methods

2.1. Materials

Coatings were deposited from, first, micrometer-sized alumina powders, and second, a water-based suspension containing submicrometer-sized alumina powder.

Metco 6103 (Oerlikon Metco, Pfäffikon, Switzerland), a commercially available α-Al_2O_3 agglomerated and sintered powder, was used to produce coatings by means of atmospheric plasma spraying (APS). The powder particle size was in the range of $-45 + 15$ µm, and the declared particle size distribution was confirmed by powder granulometry (PSA 1190, Anton Paar, Graz, Austria).

Liquid feedstock, dedicated for suspension plasma spraying (SPS) with radial injection and suspension-based high-velocity oxy-fuel spraying (S-HVOF), was formulated in-house. This was a water-based suspension produced by using the commercially available α-Al_2O_3 powder, MARTOXID® MZS-1 (Martinswerk GmbH, Bergheim, Germany), with a solid content equal to 25 wt.%. The average powder particle size was about 1.2 µm. The diameters of the fine powders were evaluated with a Litesizer 500 granulometer (Anton Paar, Graz, Austria). A detailed study on the properties of this feedstock can be found elsewhere [1].

Axially injected suspension plasma-sprayed coatings were obtained using a commercial aqueous, ready-to-spray AuerCoat® Al_2O_3 suspension (Treibacher Industrie AG, Althofen, Austria), with 40 wt.% solid content and α–Al_2O_3 submicrometer-sized powder with a d_{v50} of 2.2 µm. The powder granulometry testing results are summarized in Table 1. All feedstocks revealed a monomodal particle size distribution.

Table 1. Particle size distribution of Al_2O_3 powders used for deposition of the coatings; d_v—particle size by volume [µm]; APS—atmospheric plasma spraying, SPS—suspension plasma spraying with radial injection, A-SPS—suspension plasma spraying with axial injection.

Particle Size	Al_2O_3_APS	Al_2O_3_SPS	Al_2O_3_A-SPS	Al_2O_S-HVOF
Feedstock Type	Powder (Metco 6103)	Suspension (MSZ-1)	Suspension (AuerCoat)	Suspension (MSZ-1)
d_{v10}	20.6	0.8	0.5	0.8
d_{v50}	36.2	1.2	2.2	1.2
d_{v90}	64.6	1.8	4.9	1.8

The distribution of powder particles sizes was confirmed by FEG-SEM investigation (Leo 1530, Zeiss, Zürich, Switzerland) and SEM TESCAN VEGA 3 SBH (Tescan, Brno, Czech Republic), as shown in Figure 1.

2.2. Spraying Processes

To avoid clogging the injector nozzle during APS spraying, the micrometer-sized powder was previously dried for 2 h at 120 °C. The suspensions were redispersed by continuous mechanical stirring. The stainless-steel coupons, of 3 mm thickness and a diameter equal to 25 mm, were grit-blasted and cleaned with ethanol prior to spraying.
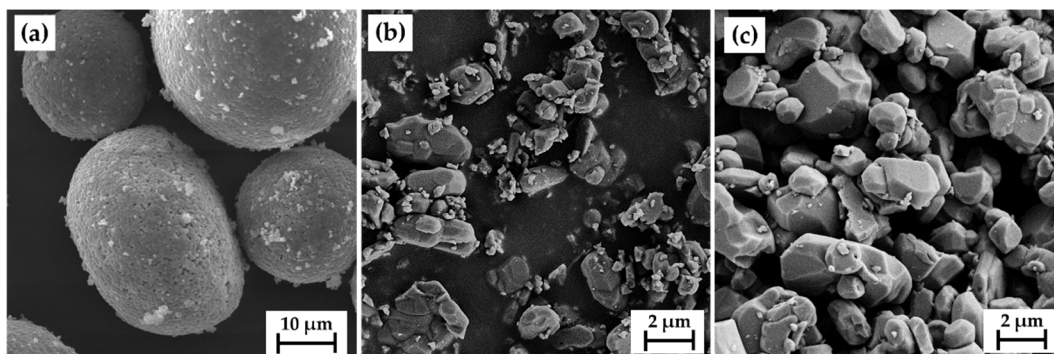
Figure 1. Morphologies of alumina feedstock powders used for spraying: (**a**) METCO 6103, (**b**) MZS-1, (**c**) dried powder of AuerCoat® suspension.

The main spraying parameters are shown in Table 2. APS spraying, performed at Wroclaw University, was carried out with one anode and one cathode SG-100 torch (Praxair, Indianapolis, IN, USA). SPS spraying with radial injection was performed at Fraunhofer IWS, using a cascaded plasma torch KK (AMT AG, Kleindöttingen, Switzerland), while A-SPS spraying using a Mettech Axial III (Northwest Mettech Corp., Vancouver, Canada) was performed at University West. In both SPS processes, the stand-off distances were similar to the powder-based APS process. S-HVOF spraying was performed at Fraunhofer IWS using an HVOF Top Gun (GTV Verschleißschutz GmbH, Luckenbach, Germany) with a modified combustion chamber that allowed internal and axial feeding of the suspension, as previously described by Toma et al. [22,25,42].

Table 2. Main spraying parameters. For each process, the most appropriate spraying conditions were chosen to produce alumina coatings that were as dense as possible.

Spray Parameter	APS	SPS	A-SPS	S-HVOF
Electrical power, kW	35	45	120	>100
Spraying gases, slpm	Ar/H_2: 45/5	Ar/H_2: 50/6	Ar/N_2/H_2: 45/45/10	C_2H_4/O_2: 75/230
Injection mode	radial	radial	axial	axial
Stand-off distance, mm	100	80	100	90
Torch passes	8	20	30	20
Powder feed rate, g/min	20	-	-	-
Suspension feed rate, mL/min	-	35	40	35
Coating thickness, μm	189 ± 24	172 ± 9	304 ± 5	200 ± 10

2.3. Coating Characterization

Microstructural characterization of the coatings' surfaces and cross-sections was carried out using the scanning electron microscopes PHENOM G2 PRO (Phenom World BV, Eindhoven, The Netherlands) and TESCAN VEGA 3 SBH (Tescan, Brno, Czech Republic). Prior to cross-sectional investigations, the metallographic preparation included precise cutting, cold mounting in low viscosity epoxy resin, grinding, end polishing, and gold sputtering. To determine the porosity of the coatings, ImageJ 1.50i software was used, and the standard procedure described by standard ASTM E2109-01(2014) was performed [43,44]. For this purpose, the cross-section micrographs were taken in at least 20 random areas.

The crystalline phases in the feedstocks and as-sprayed coatings were investigated by X-ray diffraction (XRD) using a D8 Discover diffractometer (Bruker AXS, Karlsruhe, Germany) with CuK_α radiation. The range of 2θ acquisition was 10° to 80°. The crystalline phases were identified using the JCPDS standard cards: 00-046-1212 (α-Al_2O_3) and

00-010-0425 (γ-Al$_2$O$_3$). The volume percentage of the α-Al$_2$O$_3$ and γ-Al$_2$O$_3$ phases was determined using Equation (1) (following [42]):

$$C_\gamma^{\text{Al}_2\text{O}_3} = \frac{I_\gamma(400)}{I_\alpha(113) + I_\gamma(400)} \times 100 \ [\%],\tag{1}$$

where $C_\gamma^{\text{Al}_2\text{O}_3}$ is the content of γ-Al$_2$O$_3$ phase content, and I_γ, I_α is the intensity of the peak diffraction for the corresponding plane of γ-Al$_2$O$_3$ and α-Al$_2$O$_3$, accordingly.

The microhardness was measured by Vickers indentations with 0.2 N loading, using a Sinowon HV-1000 apparatus (Sinowon Innovation Metrology, DongGuan, China). For each coating sample, 10 indentations were made.

The intensity of wear behavior and the friction coefficients of the coatings were investigated using a ball-on-disk (BOD) tribometer CSM (CSM Instruments SA, Peseux, Switzerland) in dry sliding contact conditions, at room temperature. The WC counterpart ball diameter was 6 mm with a hardness of 16 GPa, which exceeds the approximate 15 GPa of the hardness reported for alumina [45]. The test conditions were: 10 N normal load, sliding speed of 0.1 m/s, 1000 m sliding distance, and 3 mm radius of the wear track. The wear rate was calculated according to the formula given elsewhere [46,47], taking into account the material volume loss, load, and sliding distance. Prior to testing, the coatings' surfaces were ground and polished to assure the surface roughness (Ra) was below 0.2 μm, as specified by the ASTM G99 standard [48]. The morphology of the wear track was examined using a scanning electron microscope PHENOM G2 PRO (Phenom World BV, Eindhoven, The Netherlands).

3. Results and Discussion

3.1. Morphology and Microstructure

Both as-sprayed conventional APS and suspension-sprayed coatings exhibited a characteristic topography that is typical for thermally sprayed deposits (Figure 2). APS coating (Figure 2a) had some microcracks and partially melted powder particles but, generally, was built from micrometer-sized splats. Cracks emerged in the coatings due to the high energy input during spraying. Unmelted powder particles remaining in the structure were due to the residence of Al$_2$O$_3$ particles in the plasma within less than 1/1000 s [49], or from particles traveling in the external and colder plasma jet region. It was already reported [50] that in the case of agglomerated powders, such a period is not sufficient to completely melt the agglomerated powder sized 20–50 μm. It results in lower thermal conductivity when compared to the fused powder. Additionally, the radial injection meant that some powders traveled in hotter and some in colder plasma jet regions, so this causes some differences in the melting of the feedstock during spraying. In the case of suspension-based processes, the melting process of fine alumina powders is different. During injection into the plasma, they melt fully, so, basically, the structure consists of well-melted and fine splats. Some of the particles, which stay in the colder plasma regions, transform into a liquid state, but only partially. Therefore, some partially melted or re-solidified powder particles are also observed in suspension-sprayed coatings (SPS, A-SPS, and S-HVOF). However, for the same suspension feedstock, the effect was more visible when radial injection was used (SPS, Figure 2b) than in the S-HVOF process (Figure 2d). The presence of very fine particles, observed in A-SPS coatings (Figure 2c), was mainly because of the wider powder particle size distribution in the suspension, where the starting powder contained 10 vol.% of particles smaller than 0.5 μm but also because of the greater stand-off distance, which could lead to the re-solidification of the finest powder particles.
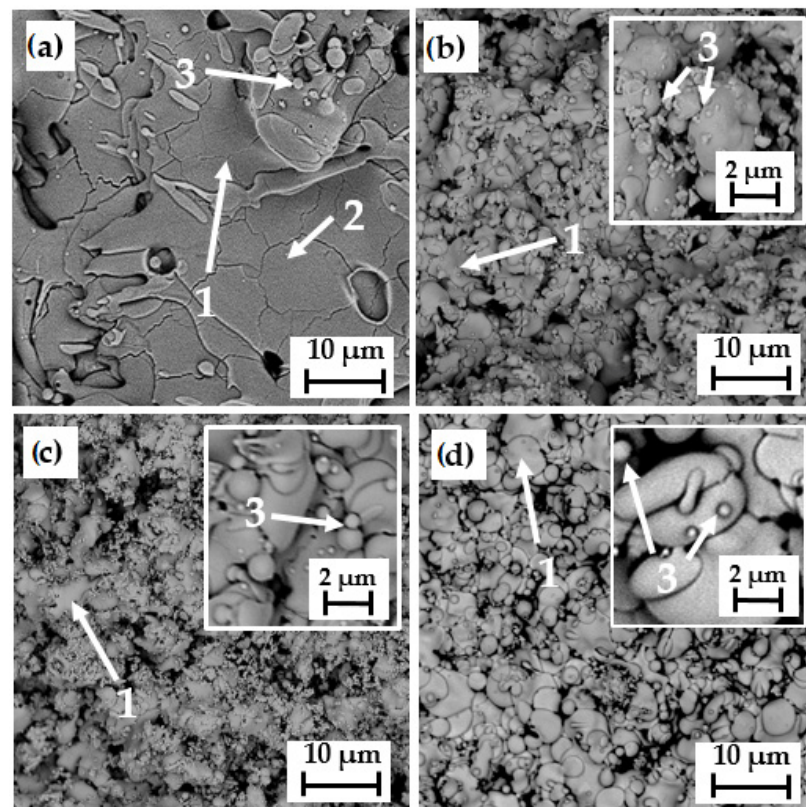
Figure 2. SEM top-surface morphologies of Al$_2$O$_3$ coatings sprayed by: (**a**) APS, (**b**) SPS, (**c**) A-SPS, and (**d**) S-HVOF. 1—splat; 2—cracks; 3—not fully melted or re-solidified particles.

Figure 3 presents cross-section SEM images of the deposited coatings. As already discussed, the splat size in conventional APS coatings was larger than in fine-grained, suspension-based ones. It was observed that the axially sprayed coatings A-SPS and S-HVOF (see Figure 3c,d) were characterized by a dense, uniform microstructure with the lowest porosity of 6 vol.% and 4 vol.%, respectively. Pores were observed mainly in the APS and SPS deposits. The main difference was in the size of the pores—although the coatings were of similar porosity (12 vol.%—APS coating; 15 vol.%—SPS coating), the pores in APS coatings were of micrometer size, while SPS coating had refined porosity.
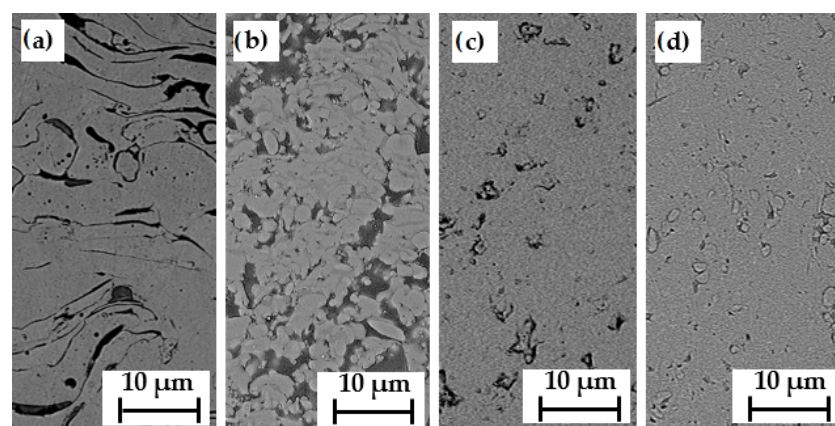

Figure 3. SEM cross-section micrographs of Al$_2$O$_3$ coatings sprayed by: (**a**) APS, (**b**) SPS, (**c**) A-SPS and (**d**) S-HVOF.

3.2. Phase Composition of Alumina Coatings

The phase analysis of all feedstock powders confirmed that in all cases, 100 vol.% rhombohedral α-Al$_2$O$_3$ phase was found (see example in Figure 4a). During the coating deposition, the γ-Al$_2$O$_3$ crystalline phase has also been formed; the ratios of α and γ alumina were different, depending on the spray method (Table 3). Such differences resulted from heat input and the mechanism of coating deposition, as well as particle heat capacity. An example XRD diffractogram obtained for S-HVOF coating is given in Figure 4b.
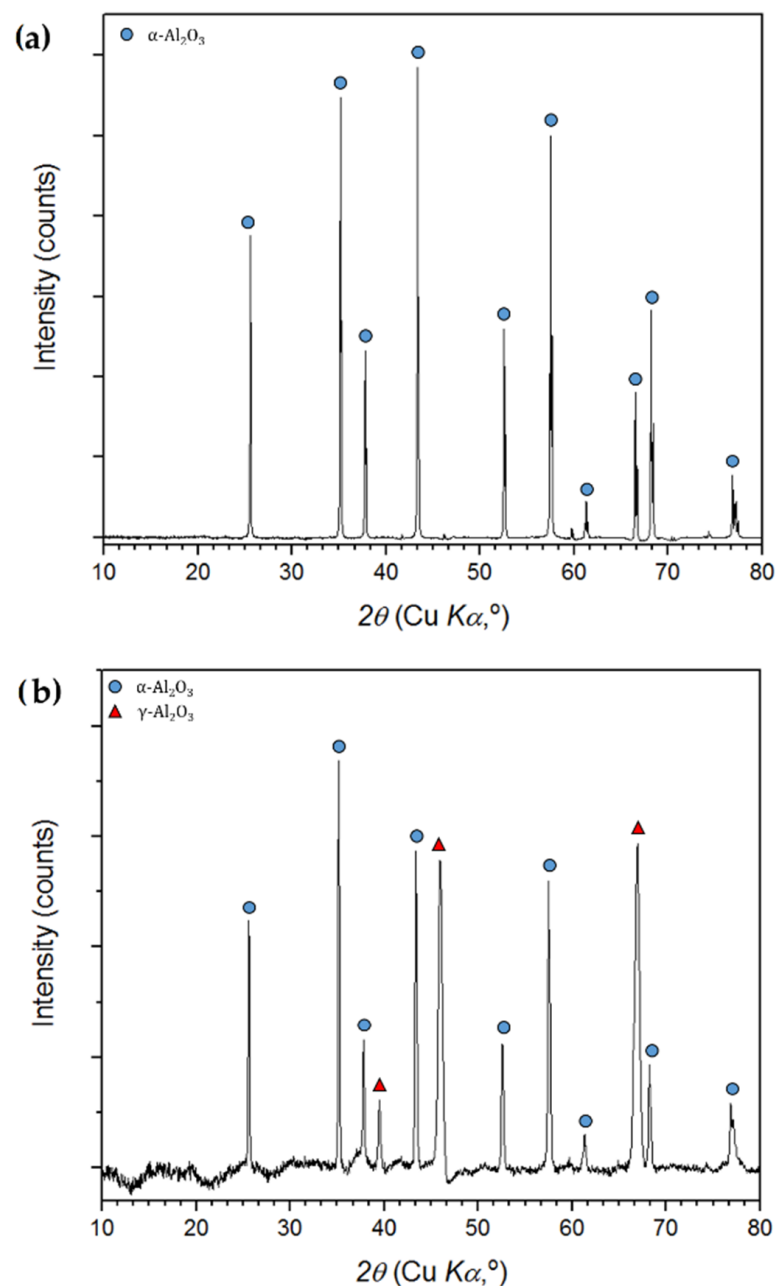

Figure 4. XRD diffractograms of (**a**) the Metco 6103 feedstock and (**b**) the manufactured coating (S-HVOF).

Table 3. Quantitative estimation of the XRD phase composition (based on Equation (1)) in coatings sprayed using different techniques.

Crystalline Phase	APS	SPS	A-SPS	S-HVOF
α-Al$_2$O$_3$ Phase, vol.%	51	63	52	55
γ-Al$_2$O$_3$ Phase, vol.%	49	37	48	45

In thermal spray coatings, due to the rapid heating and cooling of powder particles, phase transformation occurs from α to γ-Al$_2$O$_3$. This transformation is a result of the high temperature and the preferential nucleation of γ-Al$_2$O$_3$ at high cooling rates [51]. For APS coating, the quantitative results (see Table 3) are similar to the ones in the literature [25,52]. On the other hand, for SPS coating, the content of γ-Al$_2$O$_3$ was the lowest. This was probably connected with a relatively high fraction of not fully melted particles, which was caused by radial injection. In such an injection mode, there is a problem with achieving good penetration of the plasma plume by submicrometer-powder particles. Similar results could be found, for instance, in [44]. This could be explained by the two-zone microstructure of SPS coatings [53]. A higher content of α-Al$_2$O$_3$ phase in SPS coating, in comparison to the APS one, resulted also from the fact that APS particles are in direct contact with the plasma, whereas in SPS some energy is consumed by the evaporation of the liquid phase [13]. In the case of A-SPS coating, the injection mode was axial. This change resulted in better penetration of the plasma flame, reaching its hot core. Consequently, the powder particles have been exposed to a higher heat load, which resulted in a higher content of α-Al$_2$O$_3$ phase in the coating. Nevertheless, in this case, some energy was also consumed by the evaporation of the liquid phase from suspension. For S-HVOF coating, the heat treatment by flame is much lower than in the case of plasma. On the other hand, the axial injection mode promoted better particle heat treatment.

3.3. Microhardness

The microhardness of the coatings was dependent on the phase composition, the porosity, the presence of not fully melted particles, and cohesion (Figure 5). In general, a coating that contains non-melted powders may exhibit either lower microhardness (because of poor interlamellar bonding), or higher microhardness, resulting from the retained α phase [49]. APS coatings exhibit relatively high values of microhardness (see Figure 5). This could be related to a rather dense structure and good interlamellar cohesion. Similar results could be found, e.g., in [54]. For SPS coating, the non-homogeneous microstructure plays an important role in the microhardness value. The porosity is the highest among all tested samples (15 vol.%). There is a high number of non-melted and re-solidified particles, which weaken the coating. However, taking into account such defects, the microhardness value is still relatively high. Similar results are mentioned by [55]. In the case of A-SPS coating, in this structure, many re-solidified particles could be observed. Moreover, the much smaller size of splats and pores means that the indent spans several splats. This phenomenon [56] could decrease the real microhardness value (see Figure 5), but it is still in accordance with the literature [32]. The highest values of microhardness were obtained for S-HVOF coating. This could be explained by coating giving the most compact microstructure, the lowest porosity level (only 4 vol.%), and very strong interlamellar cohesion. Moreover, small pores are homogeneously distributed within the coatings, which do not greatly affect the microhardness, as is in line with other reported findings [57].
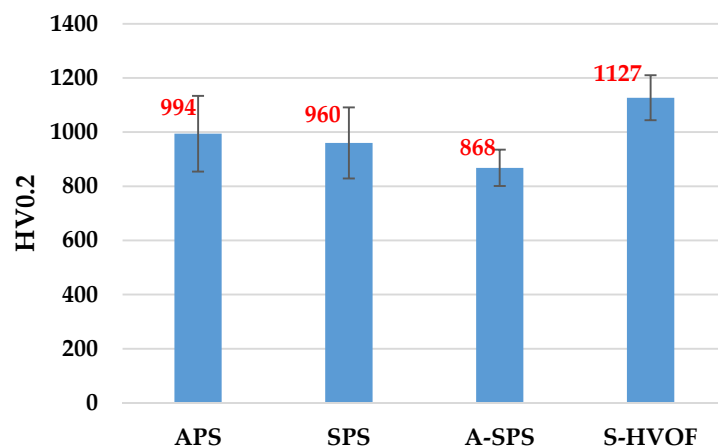
Figure 5. Vickers' microhardness of deposited Al_2O_3 coatings.

3.4. Wear Behavior

The sliding wear results given in Figure 6 present the wear rate and coefficient of friction (COF) of the suspension-sprayed and conventionally deposited alumina coatings. Comparative analysis indicates the superior wear resistance of S-HVOF coating, which presents a negligible wear rate, equal to 0.2 ± 0.04 mm$^3 \times 10^{-6}$/(N·m). This was one order of magnitude lower than A-SPS coating, and about two orders of magnitude lower than the wear rate of APS coating.
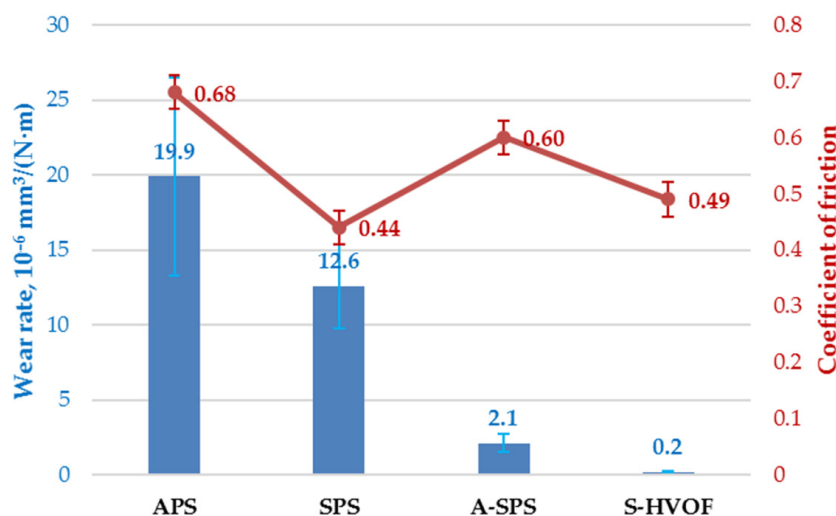

Figure 6. Wear rate and friction coefficient of different techniques for sprayed alumina coatings.

It is known that hardness is a major factor influencing the wear resistance of solid materials [58], therefore the superior anti-wear properties of S-HVOF coatings derive mainly from the highest hardness of S-HVOF-deposited alumina (average value of 1127 HV0.2 (see Figure 5)), which exceeds the hardness of other samples. Moreover, in the case of thermally deposited ceramic materials, their characteristic microstructural features, likewise their porosity, lamellar microstructure, interlamellar bonding, or various discontinuities, affect the wear behavior. In the case of A-SPS coating, the axial injection of the suspension resulted in a compact microstructure with high wear resistance, despite a lower hardness value.

The dominant wear mechanism of APS coating was fatigue-induced delamination of the splat material and subsequent adhesive smearing debris. The material loss was caused by delamination, initiated at fatigue cracks, pores, and the splat border. The coefficients of friction (COF) of the coatings are comparable to the values reported in the literature [32,54]. In addition, wear investigation confirms the higher COF of APS and A-SPS coatings than

in those deposited by the SPS and S-HVOF processes. The α-Al$_2$O$_3$ is characterized by higher toughness than that reported for the γ-Al$_2$O$_3$ phase [59], therefore the S-HVOF coating, which is α-Al$_2$O$_3$-enriched, presents superior hardness; this explains the beneficial frictional behavior. Undoubtedly, the microstructure, cohesion, splat size, and occurrence of defects such as cracks and pores affect the wear mechanisms of ceramic materials [60]. Therefore, the lowest average COF of SPS coating can be explained by the reduction of friction, due to the smearing action of the fine and loosely worn debris. Hence, even SPS coating has a relatively high mass loss; however, it exhibits a low coefficient of friction.

Although all ceramic coatings presented the adhesive wear mode supported by the fatigue-induced material delamination, their overall wear mechanism was different, see Figure 7. In all coating wear tracks, the presence of wear debris and tribofilm was identified. Similar findings were already mentioned in our previous study [39], in which both the wear of the WC counterpart and debris material transfer of the alumina coatings/counterpart ball were identified. This was also proved in this work by the SEM-EDS investigation of the tribofilm. Transfer of the counter ball material into the wear debris was confirmed by the presence of tungsten in the wear track (25.3 $\pm$ 2.8 wt.% W). Although, the identified tungsten content in tribofilm was at a comparable level, with a relatively low standard deviation (the mean tribofilm's chemical composition in wt.% is: O = 35.8 $\pm$ 2.5; Al = 27.7 $\pm$ 2.2; W = 25.3 $\pm$ 2.8; and N = 11.2 $\pm$ 0.7). Coating wear behavior was affected by the deposition technique and process parameters themselves. APS coating had severe adhesive wear, followed by grooving wear and delamination of the material, which relies on the brittle mode (the presence of cracks). APS coating's microstructural non-uniformities, such as initial cracks, the lamellar microstructure, and porosity, facilitating material loss were confirmed in the previous work [39]. On the other hand, SPS coating presented the adhesive transfer of coating material, strongly influenced by poor coating cohesion (see Figure 7c). SPS deposited coatings had better wear performance than APS ones, because of the transfer of fine wear debris along the wear track. It mitigated the COF and wear rate when compared to APS coatings. Furthermore, the A-SPS coating wear mechanism presented in Figure 7e,f had the adhesive behavior, the tribofilm was transferred through the wear track, and cyclic fatigue resulted in coating material delamination. Wear debris were uniformly smashed at the edges of the wear track where underwent moderate grooving wear. This dense tribofilm was beneficial until it was removed due to fatigue-induced cracking. In the case of S-HVOF coating (Figure 7g,h), the wear was greatly reduced when compared to other investigated coatings. It derives from the superior properties of S-HVOF coating, likewise the high adhesion [1], dense morphology and microstructure, lack of cracks, pores or other discontinuities, which support the superior antifatigue performance of S-HVOF alumina coating. After testing, the surface material loss was negligible and decreased the surface roughness in the wear track area. The obtained wear debris was preserved in the roughness pits and scratches. The adhesive smashing of debris, produced by the cutting of the surface heights and fatigue-delaminated coating material, was observed. The compact tribofilm was formed. Following the findings of Bolelli et al. [52], it can be claimed that the formation of a compact film visible at the edges of the wear track of A-SPS and S-HVOF supported the anti-wear alumina properties. Finally, it should be pointed out that the dense, tough, and uniform structure likewise manufactured by the A-SPS and S-HVOF processes, followed by the dense tribofilm formation, mitigated the adhesive wear mechanism of alumina coatings, and was beneficial for their tribological performance. The obtained findings confirmed that, among the four investigated alumina coatings, the S-HVOF sprayed ones were characterized by the most favorable wear behavior.

The results clearly showed that the wear behavior of alumina coatings is strongly determined by the size of the feedstock material and the spray process itself.
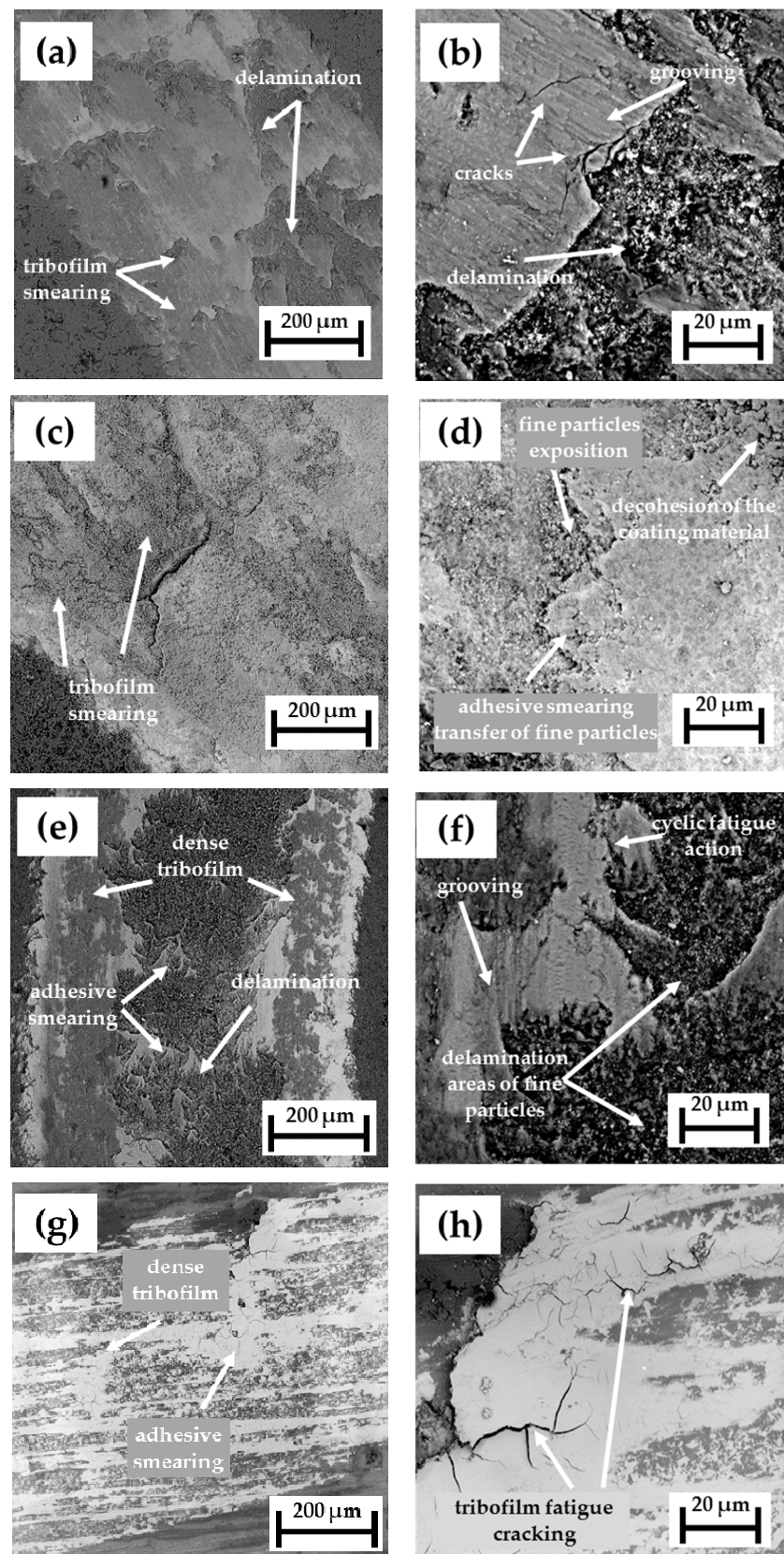
Figure 7. The wear traces of different alumina coatings, deposited using: (**a**,**b**) APS; (**c**,**d**) SPS; (**e**,**f**) A-SPS; (**g**,**h**) S-HVOF techniques.

4. Conclusions

In this work, the microstructure and tribological behavior of conventional (APS) and fine-grained suspension sprayed (SPS, A-SPS, and S-HVOF) Al_2O_3 coatings have been investigated. The following conclusions can be drawn.

All as-sprayed alumina coatings were fairly uniformly built and showed a typical lamellar morphology, even for suspension-sprayed coatings obtained at rather long spray distances (90 or 100 mm). The typical microstructural features (i.e., the size of lamellas, the number of non-melted or resolidified powder particles embedded in the structure, the size and volume of pores and microcracks) were mainly influenced by the type of feedstock used for spraying (coarse vs. fine powders), the injection mode used (radial vs axial), and the spray process characteristic (plasma spraying vs. HVOF). The use of suspension feedstock, together with axial injection (S-HVOF and A-SPS), resulted in homogeneous, fine-grained, and dense coatings.

The phase composition was strongly affected by the deposition process (heat input for plasma and flame) as well as spray parameters. The axial injection mode promoted a higher amount of α-Al_2O_3 phase.

In the case of microhardness values, the microstructure played an important role. The highest value was exhibited by S-HVOF coating (1127 HV0.2). This could be related to the low porosity, high interlamellar cohesion, and limited presence of non-melted and re-solidified particles in the coating.

The wear rate of finely grained coatings sprayed from suspensions (SPS, A-SPS, and S-HVOF) is lower than that reported for APS powder deposits. The results indicate the superior wear resistance of S-HVOF coating, which presents a negligible wear rate, equal to 0.2 ± 0.04 mm^3 $\times 10^{-6}$/(N·m). This wear rate was one order of magnitude lower than that for A-SPS coating, and almost two orders of magnitude lower than the wear rate for APS coating.

The wear mechanism of ceramic coatings includes the adhesive wear mode supported by the fatigue-induced material delamination. Moreover, the presence of wear debris and tribofilm was confirmed. S-HVOF and axial suspension plasma spraying (A-SPS) allow the deposition of dense and coherent coatings, which mitigates the adhesive action and reduces the coating material mass loss.

The lowest average COF values of 0.44 and 0.49 were obtained for SPS and S-HVOF sprayed coatings, respectively. In the case of SPS coating, this can be explained by the reduction of friction due to the smearing action of the fine and loosely worn debris, while for S-HVOF, this was an effect of the high coating hardness mitigating the adhesive wear mechanism.

References

1. Michalak, M.; Latka, L.; Sokolowski, P.; Toma, F.-L.; Myalska, H.; Denoirjean, A.; Ageorges, H. Microstructural, mechanical and tribological properties of finely grained Al_2O_3 coatings obtained by SPS and S-HVOF methods. *Surf. Coat. Technol.* **2020**, *404*, 126463. [CrossRef]

2. Grimm, M.; Conze, S.; Berger, L.-M.; Paczkowski, G.; Lindner, T.; Lampke, T. Microstructure and sliding wear resistance of plasma sprayed Al_2O_3-Cr_2O_3-TiO_2 ternary coatings from blends of single oxides. *Coatings* **2020**, *10*, 42. [CrossRef]

3. Pandey, S.; Bansal, A.; Omer, A.; Singla, A.K.; Goyal, D.K.; Singh, J.; Gupta, M.K. Effect of fuel pressure, feed rate, and spray distance on cavitation erosion of rodojet sprayed Al_2O_3 + 50% TiO_2 coated AISI410 steel. *Surf. Coat. Technol.* **2021**, 126961. [CrossRef]

4. Korkut, E.; Atlar, M. An experimental investigation of the effect of foul release coating application on performance, noise and cavitation characteristics of marine propellers. *Ocean. Eng.* **2012**, *41*, 1–12. [CrossRef]

5. Liu, Y.; Fischer, T.E.; Dent, A. Comparison of HVOF and plasma-sprayed alumina/titania coatings—Microstructure, mechanical properties and abrasion behavior. *Surf. Coat. Technol.* **2003**, *167*, 68–76. [CrossRef]

6. Tomaszek, R.; Pawlowski, L.; Zdanowski, J.; Grimblot, J.; Laureyns, J. Microstructural transformations of TiO_2, Al_2O_3 + 13 TiO_2 and Al_2O_3 + 40 TiO_2 at plasma spraying and laser engraving. *Surf. Coat. Technol.* **2004**, *185*, 137–149. [CrossRef]

7. Bolelli, G.; Lusvarghi, L.; Manfredini, T.; Pighetti Mantini, F.; Turunen, E.; Varis, T.; Hannula, S.-P. Comparison between plasma- and HVOF-sprayed ceramic coatings. Part II: Tribological Behaviour. *Int. J. Surf. Sci. Eng.* **2007**, *1*. [CrossRef]

8. Michalak, M.; Łatka, L.; Sokołowski, P.; Niemiec, A.; Ambroziak, A. The microstructure and selected mechanical properties of Al_2O_3 + 13 wt.% TiO_2 plasma sprayed coatings. *Coatings* **2020**, *10*, 173. [CrossRef]

9. Ageorges, H.; Ctibor, P. Comparison of the structure and wear resistance of Al_2O_3–13 wt.%TiO_2 coatings made by GSP and WSP plasma process with two different powders. *Surf. Coat. Technol.* **2008**, *202*, 4362–4368. [CrossRef]

10. Szala, M.; Dudek, A.; Maruszczyk, A.; Walczak, M.; Chmiel, J.; Kowal, M. Effect of atmospheric plasma sprayed TiO_2-10% NiAl cermet coating thickness on cavitation erosion, sliding and abrasive wear resistance. *Acta Phys. Pol. A* **2019**, *136*, 335–341. [CrossRef]

11. Wang, Y.; Stella, J.; Darut, G.; Poirier, T.; Liao, H.; Planche, M.-P. APS Prepared NiCrBSi-YSZ composite coatings for protection against cavitation erosion. *J. Alloys Compd.* **2017**, *699*, 1095–1103. [CrossRef]

12. Iqbal, A.; Siddique, S.; Maqsood, M.; Atiq Ur Rehman, M.; Yasir, M. Comparative analysis on the structure and properties of iron-based amorphous coating sprayed with the thermal spraying techniques. *Coatings* **2020**, *10*, 1006. [CrossRef]

13. Gopal, V.; Goel, S.; Manivasagam, G.; Joshi, S. Performance of hybrid powder-suspension axial plasma sprayed Al_2O_3-YSZ coatings in bovine serum solution. *Materials* **2019**, *12*, 1922. [CrossRef] [PubMed]

14. Khosravifard, A.; Salahinejad, E.; Yaghtin, A.H.; Araghi, A.; Akhbarizadeh, A. Tribochemical behavior of alumina coatings deposited by high-velocity oxy fuel spraying. *Ceram. Int.* **2015**, *41*, 5713–5720. [CrossRef]

15. Myalska, H.; Lusvarghi, L.; Bolelli, G.; Sassatalli, P.; Moskal, G. Tribological behavior of WC-Co HVAF-sprayed composite coatings modified by nano-sized TiC addition. *Surf. Coat. Technol.* **2019**, *371*, 401–416. [CrossRef]

16. Kiilakoski, J.; Langlade, C.; Koivuluoto, H.; Vuoristo, P. Characterizing the micro-impact fatigue behavior of APS and HVOF-sprayed ceramic coatings. *Surf. Coat. Technol.* **2019**, *371*, 245–254. [CrossRef]

17. Bolelli, G.; Lusvarghi, L.; Varis, T.; Turunen, E.; Leoni, M.; Scardi, P.; Azanza-Ricardo, C.L.; Barletta, M. Residual stresses in HVOF-sprayed ceramic coatings. *Surf. Coat. Technol.* **2008**, *202*, 4810–4819. [CrossRef]

18. Szala, M.; Walczak, M.; Łatka, L.; Gancarczyk, K.; Özkan, D. Cavitation erosion and sliding wear of MCrAlY and NiCrMo coatings deposited by HVOF thermal spraying. *Adv. Mater. Sci.* **2020**, *20*, 26–38. [CrossRef]

19. Mousavi, S.E.; Naghshehkesh, N.; Amirnejad, M.; Shammakhi, H.; Sonboli, A. Wear and corrosion properties of stellite-6 coating fabricated by HVOF on nickel–aluminium bronze substrate. *Met. Mater. Int.* **2020**. [CrossRef]

20. Zhou, Y.; Kang, J.; Yue, W.; Liu, X.; Fu, Z.; Zhu, L.; She, D.S.; Ma, G.; Wang, H. Sliding wear properties of HVOF sprayed WC-10Co4Cr coatings with conventional structure and bimodal structure under different loads. *J. Tribol.* **2021**, 1–29. [CrossRef]

21. Jonda, E.; Łatka, L.; Pakieła, W. Microstructure and selected properties of Cr_3C_2–NiCr coatings obtained by HVOF on magnesium alloy substrates. *Materials* **2020**, *13*, 2775. [CrossRef]

22. Toma, F.-L.; Berger, L.-M.; Scheitz, S.; Langner, S.; Rödel, C.; Potthoff, A.; Sauchuk, V.; Kusnezoff, M. Comparison of the microstructural characteristics and electrical properties of thermally sprayed Al_2O_3 coatings from aqueous suspensions and feedstock powders. *J. Therm. Spray Tech.* **2012**, *21*, 480–488. [CrossRef]

23. Bolelli, G.; Bonferroni, B.; Cannillo, V.; Gadow, R.; Killinger, A.; Lusvarghi, L.; Rauch, J.; Stiegler, N. Wear behaviour of high velocity suspension flame sprayed (HVSFS) Al_2O_3 coatings produced using micron- and nano-sized powder suspensions. *Surf. Coat. Technol.* **2010**, *204*, 2657–2668. [CrossRef]

24. Killinger, A. 4 Status and future trends in suspension spray techniques. In *Future Development of Thermal Spray Coatings*; Espallargas, N., Ed.; Woodhead Publishing: Sawston, UK, 2015; pp. 81–122, ISBN 978-0-85709-769-9.

25. Michalak, M.; Toma, F.-L.; Latka, L.; Sokolowski, P.; Barbosa, M.; Ambroziak, A. A study on the microstructural characterization and phase compositions of thermally sprayed Al_2O_3-TiO_2 coatings obtained from powders and water-based suspensions. *Materials* **2020**, *13*, 2638. [CrossRef]

26. Rauch, J.; Bolelli, G.; Killinger, A.; Gadow, R.; Cannillo, V.; Lusvarghi, L. Advances in high velocity suspension flame spraying (HVSFS). *Surf. Coat. Technol.* **2009**, *203*, 2131–2138. [CrossRef]

27. Mahade, S.; Björklund, S.; Govindarajan, S.; Olsson, M.; Joshi, S. Novel wear resistant carbide-laden coatings deposited by powder-suspension hybrid plasma spray: Characterization and testing. *Surf. Coat. Technol.* **2020**, *399*, 126147. [CrossRef]

28. Vargas, F.; Ageorges, H.; Fournier, P.; Fauchais, P.; Lopez, M.E. Mechanical and tribological performance of Al$_2$O$_3$-TiO$_2$ Coatings elaborated by flame and plasma spraying—ScienceDirect. *Surf. Coat. Technol.* **2010**, *205*, 1132–1136. [CrossRef]

29. Goel, S.; Björklund, S.; Curry, N.; Govindarajan, S.; Wiklund, U.; Gaudiuso, C.; Joshi, S. Axial plasma spraying of mixed suspensions: A case study on processing, characteristics, and tribological behavior of Al$_2$O$_3$-YSZ coatings. *Appl. Sci.* **2020**, *10*, 5140. [CrossRef]

30. Björklund, S.; Goel, S.; Joshi, S. Function-dependent coating architectures by hybrid powder-suspension plasma spraying: Injector design, processing and concept validation. *Mater. Des.* **2018**, *142*, 56–65. [CrossRef]

31. Ganvir, A.; Curry, N.; Björklund, S.; Markocsan, N.; Nylén, P. Characterization of microstructure and thermal properties of YSZ Coatings obtained by axial suspension plasma spraying (ASPS). *J. Therm. Spray Tech.* **2015**, *24*, 1195–1204. [CrossRef]

32. Goel, S.; Björklund, S.; Curry, N.; Wiklund, U.; Joshi, S. Axial suspension plasma spraying of Al$_2$O$_3$ coatings for superior tribological properties. *Surf. Coat. Technol.* **2017**, *315*, 80–87. [CrossRef]

33. Marcinauskas, L.; Mathew, J.S.; Milieška, M.; Thanigachalam, B.; Kupec, A.; Česnavičius, R.; Kėželis, R.; Kalin, M. Microstructure and tribological properties of plasma sprayed alumina and alumina-graphite coatings. *Surf. Coat. Technol.* **2018**, *350*, 401–409. [CrossRef]

34. Darut, G.; Ageorges, H.; Denoirjean, A.; Montavon, G.; Fauchais, P. Effect of the structural scale of plasma-sprayed alumina coatings on their friction coefficients. *J. Therm. Spray Tech.* **2008**, *17*, 788–795. [CrossRef]

35. Rico, A.; Rodriguez, J.; Otero, E.; Zeng, P.; Rainforth, W.M. Wear behaviour of nanostructured alumina–titania coatings deposited by atmospheric plasma spray. *Wear* **2009**, *267*, 1191–1197. [CrossRef]

36. Praveen, A.S.; Arjunan, A. Parametric optimisation of high-velocity oxy-fuel nickel-chromium-silicon-boron and aluminium-oxide coating to improve erosion wear resistance. *Mater. Res. Express* **2019**, *6*, 096560. [CrossRef]

37. Szala, M.; Łatka, L.; Awtoniuk, M.; Winnicki, M.; Michalak, M. Neural modelling of APS thermal spray process parameters for optimizing the hardness, porosity and cavitation erosion resistance of Al$_2$O$_3$-13 wt.% TiO$_2$ coatings. *Processes* **2020**, *8*, 1544. [CrossRef]

38. Taltavull, C.; Lopez, A.J.; Torres, B.; Atrens, A.; Rams, J. Optimisation of the high velocity oxygen fuel (HVOF) parameters to produce effective corrosion control coatings on AZ91 magnesium alloy. *Mater. Corros.* **2015**, *66*, 423–433. [CrossRef]

39. Łatka, L.; Michalak, M.; Szala, M.; Walczak, M.; Sokołowski, P.; Ambroziak, A. Influence of 13 wt.% TiO$_2$ content in alumina-titania powders on microstructure, sliding wear and cavitation erosion resistance of APS sprayed coatings. *Surf. Coat. Technol.* **2021**, *410*, 126979. [CrossRef]

40. Perumal, G.; Geetha, M.; Asokamani, R.; Alagumurthi, N. Wear studies on plasma sprayed Al$_2$O$_3$–40 wt.% 8YSZ composite ceramic coating on Ti–6Al–4V alloy used for biomedical applications. *Wear* **2014**, *311*, 101–113. [CrossRef]

41. Ganvir, A.; Goel, S.; Govindarajan, S.; Jahagirdar, A.R.; Björklund, S.; Klement, U.; Joshi, S. Tribological performance assessment of Al$_2$O$_3$-YSZ composite coatings deposited by hybrid powder-suspension plasma spraying. *Surf. Coat. Technol.* **2021**, *409*, 126907. [CrossRef]

42. Toma, F.-L.; Berger, L.-M.; Stahr, C.C.; Naumann, T.; Langner, S. Microstructures and functional properties of suspension-sprayed Al$_2$O$_3$ and TiO$_2$ coatings: An overview. *J. Therm. Spray Tech.* **2010**, *19*, 262–274. [CrossRef]

43. ASTM E2109-01. *Standard Test Methods for Determining Area Percentage Porosity in Thermal Sprayed Coatings*; ASTM International: West Conshohocken, PA, USA, 2014.

44. Michalak, M.; Łatka, L.; Szymczyk, P.; Sokołowski, P. Computational image analysis of suspension plasma sprayed YSZ coatings. *ITM Web Conf.* **2017**, *15*, 06004. [CrossRef]

45. Jahanmir, S. Wear of Ceramics. In *Wear—Materials, Mechanisms and Practice*; John Wiley & Sons, Ltd.: Hoboken, NJ, USA, 2005; pp. 167–189, ISBN 978-0-470-01702-9.

46. Drozd, K.; Walczak, M.; Szala, M.; Gancarczyk, K. Tribological behavior of AlCrSiN-coated tool steel K340 versus popular tool steel grades. *Materials* **2020**, *13*, 4895. [CrossRef]

47. Łatka, L.; Szala, M.; Macek, W.; Branco, R. Mechanical properties and sliding wear resistance of suspension plasma sprayed YSZ coatings. *Adv. Sci. Technol. Res. J.* **2020**, *14*, 307–314. [CrossRef]

48. ASTM E2546-15. *Standard Practice for Instrumented Indentation Testing*; ASTM International: West Conshohocken, PA, USA, 2015.

49. Singh, V.P.; Sil, A.; Jayaganthan, R. A study on sliding and erosive wear behaviour of atmospheric plasma sprayed conventional and nanostructured alumina coatings. *Mater. Des.* **2011**, *32*, 584–591. [CrossRef]

50. Zhang, J.; He, J.; Dong, Y.; Li, X.; Yan, D. Microstructure characteristics of Al$_2$O$_3$–13 wt.% TiO$_2$ coating plasma spray deposited with nanocrystalline powders. *J. Mater. Process. Technol.* **2008**, *197*, 31–35. [CrossRef]

51. Shaw, L.L.; Goberman, D.; Ren, R.; Gell, M.; Jiang, S.; Wang, Y.; Xiao, T.; Strutt, P. The dependency of microstructure and properties of nanostructured coatings on plasma spray conditions. *Surf. Coat. Technol.* **2000**, *130*, 1–8. [CrossRef]

52. Franco, D.; Ageorges, H.; Lopez, E.; Vargas, F. Tribological performance at high temperatures of alumina coatings applied by plasma spraying process onto a refractory material. *Surf. Coat. Technol.* **2019**, *371*, 276–286. [CrossRef]

53. Kozerski, S.; Pawlowski, L.; Jaworski, R.; Roudet, F.; Petit, F. Two zones microstructure of suspension plasma sprayed hydroxyapatite coatings. *Surf. Coat. Technol.* **2010**, *204*, 1380–1387. [CrossRef]

54. Bolelli, G.; Cannillo, V.; Lusvarghi, L.; Manfredini, T. Wear behaviour of thermally sprayed ceramic oxide coatings. *Wear* **2006**, *261*, 1298–1315. [CrossRef]

55. Tesar, T.; Musalek, R.; Medricky, J.; Kotlan, J.; Lukac, F.; Pala, Z.; Ctibor, P.; Chraska, T.; Houdkova, S.; Rimal, V.; et al. Development of suspension plasma sprayed alumina coatings with high enthalpy plasma torch. *Surf. Coat. Technol.* **2017**, *325*, 277–288. [CrossRef]

56. Zois, D.; Lekatou, A.; Vardavoulias, M. A Comparative Microstructural investigation of nanostructured and conventional Al$_2$O$_3$ coatings deposited by plasma spraying | SpringerLink. *J. Therm. Spray Tech.* **2008**, 887–894. [CrossRef]

57. Murray, J.W.; Ang, A.S.M.; Pala, Z.; Shaw, E.C.; Hussain, T. Suspension high velocity oxy-fuel (SHVOF)-sprayed alumina coatings: Microstructure, nanoindentation and wear. *J. Therm. Spray Tech.* **2016**, *25*, 1700–1710. [CrossRef]

58. Wen, S.; Huang, P. *Principles of Tribology*, 1st ed.; Wiley: Hoboken, NJ, USA, 2012; ISBN 978-1-118-06289-0.

59. Niu, B.; Qiang, L.; Zhang, J.; Zhang, F.; Hu, Y.; Chen, W.; Liang, A. Plasma sprayed α-Al$_2$O$_3$ main phase coating using γ-Al$_2$O$_3$ powders. *Surf. Eng.* **2019**, *35*, 801–808. [CrossRef]

60. Gahr, K.-H.Z. *Microstructure and Wear of Materials*; Elsevier: Amsterdam, The Netherlands, 1987; ISBN 978-0-08-087574-3.